Bulgarian Chemical Communications, Volume 52, Issue 4 (pp. 440-447) 2020 *DOI: 10.34049/bcc.52.4.5234*

Spectroscopic (FT-IR & FT-Raman), Fukui function and molecular docking analysis of 6-amino-7,9-dihydropurine-8-thione by DFT approach

P. Chakkaravarthy[1], V. Vetrivelan[2*], S. Syed Shafi[3], S. Muthu[4]

[1]*Department of Chemistry, Government Thirumagal Mills College Gudiyattam, Tamilnadu, India*
[2]*Department of Physics, Thanthai Periyar Government Institute of Technology, Vellore, Tamilnadu, India*
[3]*Department of Chemistry, Thiruvalluvar University, Vellore, Tamilnadu India*
[4] *Department of Physics, Aringar Anna Govt Arts College, Cheyyar, Tamilnadu, India*

Received: February 14, 2020; Revised: July 28, 2020

The title compound 6-amino-7,9-dihydropurine-8-thione (ADHPT) was analyzed using FT-IR and FT-Raman spectroscopy. The fundamental vibrational wavenumbers, IR and Raman intensities for the optimized structure of the investigated molecule were calculated and compared with the experimental vibrational spectra. The vibrational assignment of the molecule was done using potential energy distribution analysis. The electron density-based local reactivity descriptor such as Fukui function was calculated in order to explain the chemical selectivity of the reactive site in ADHPT. Frontier molecular orbitals are also reported. The MEP map was used to detect the possible electrophilic and nucleophilic sites in the molecule. All the calculations were carried out by the B3LYP/6-311++G (d,p) method. To assess the biological activity of ADHPT, molecular docking was done to recognize the hydrogen bond lengths and binding energy with antibacterial protein (5MLA – human RAS protein).

Keywords: FTIR; FT-Raman; DFT; HOMO -LUMO; Fukui function; Molecular docking

INTRODUCTION

Despite the enormous progress in medicinal chemistry, communicable diseases continue to be a major threat to our society and have provided a new challenge to researchers worldwide. The new molecular manipulation aims to approach the development of new drugs. Among various diseases, malaria and microbial infections are the widest spreading in nature. As a result, antimicrobial studies are the best way to overcome microbial resistance and to develop effective therapies. Our title compound consists of the distinctive moieties purine and thione. The title compound ADHPT and its derivatives have been studied by Gunasekaran *et al.* [1] and Latosinska *et al.* in recent years [2]. Literature survey reveals that to the best of our knowledge no DFT wavenumber calculations, complete vibrational analysis and molecular properties of ADHPT have been reported so far. In the present work, we reported a detailed theoretical and experimental vibrational spectral investigation of the given molecule with a view to identify the various normal modes with greater wavenumber accuracy. In addition, Fukui function, HOMO-LUMO, MEP and molecular docking studies were calculated. The title compound and its derivatives possess high biological activity as anti-cancer, lymphoblastic leukemia drugs, against malignancies, inflammatory bowel disease, rheumatic diseases, dermatologic conditions and solid organ transplant rejection. Their incorporation into the DNA to bring about a cytotoxic effect and their pharmacokinetics have been examined in several studies [3-5]. Previous studies revealed the ability of inhibiting the above-said diseases; in addition to that the title compound inhibits the antibacterial diseases with a higher potential compared to the purine and thione derivatives of previously synthesized compounds.

Vibrational spectroscopy is highly sensitive to structural changes and is useful for the study of pharmacological properties [6]. Thus, in order to understand the relationship between molecular structure and biological activity, the knowledge of the electronic structure and the complete vibrational spectra is mostly significant. Information about the geometry and structure of the molecule and its electrostatic potential surfaces, together with a complete analysis of the vibrational spectra using Raman and infrared techniques, based on frequency, intensity and potential energy distribution over the internal coordinates helps in understanding the structural and spectral characteristics, by allowing to obtain both qualitative and quantitative understanding of energy distribution. DFT calculations have been individually performed, as they form the basis of the assignment of the vibrational spectrum. In addition, intra- and intermolecular interactions are analyzed by different techniques, e.g. NBO analysis.

* To whom all correspondence should be sent:
E-mail: vetri.tpgit@gmail.com

The frontier molecular orbital theory is employed to predict the molecule reactivity. The complete assignments of experimental IR and Raman spectra were performed by comparison of experimental IR and Raman spectra with the corresponding theoretical ones based on the potential energy distribution (PED) and the normal internal coordinates of the ADHPT species. The treatment of solvated systems was an issue which we were unable to address. Dougherty *et al*., [6] argued that different solvation-desolvation effects will be minor if the ion is held constant while the neutral host is varied, and that gas phase calculations may therefore be of value for prediction of solution phase binding preferences. Molecular dynamics simulations in solvent boxes have proved to be successful and are undoubtedly most promising.

Owing to the increased resistance to the available drugs by antimicrobial pathogens it is essential to synthesize new drugs. According to literature, the title compound consists of effective antimicrobial moieties.

The extensive use of common antibiotics leads to a growing number of defiant bacteria through gene transfer and mutation. Based on pharmacological investigation, *in silico* binding mode of ADHPT ligand to the human RAS protein (5MLA) was also investigated by a docking procedure in this paper.

As the potential applications of the title compound evidence its biological and medicinal importance, so we carried out this study.

MATERIAL AND METHODS

Experimental details

6-Amino-7,9-dihydropurine-8-thione (ADHPT) was purchased from Sigma–Aldrich chemical company with a stated purity of 97% and was used without further purification. The FT-IR spectrum of the sample was recorded in the region of 4000–450 cm^{-1} in a KBr pellet using Spectrum Two FT-IR/Sp10 Perkin Elmer FT-IR spectrometer. The resolution of the spectrum was 4 cm^{-1}. The FT-Raman spectrum was obtained in the range of 4000–100 cm^{-1} using Bruker RFS 100/S FT-Raman spectrophotometer with a 1064 nm Nd: YAG laser source of 100 mW power.

Computational details

The optimized geometrical parameters were used in the vibrational frequency computations at the DFT levels to describe all stationary points as minima. At the optimized structure of the studied species, no imaginary frequency modes were obtained proving that a true minimum on the potential energy surface was found. We have used the gradient-corrected density functional theory [7] with a three-parameter hybrid functional (B3) [8] for the exchange part and the Lee–Yang–Parr (LYP) correlation function [9], accepted as a cost-effective approach for the computation of molecular structure, vibrational frequencies and energies of optimized structures.

By connecting the outcome of the Gauss view program [10] with symmetry considerations, assignments of vibrational frequency were finished with a high degree of accuracy. Then, the spectra were analyzed with respect to potential energy distribution (PED) contributions by the Vibrational Energy Distribution Analysis (VEDA) program [11]. Finally, the calculated normal mode vibrational frequencies provide thermodynamic properties by the way of statistical mechanics. We have scaled the numbers with a standard scaling factor 0.961 [12] to compensate for the errors originating from the basis set in completeness and avoid vibrational anharmonicity, because in the experimental method the compound is analyzed in solid phase whereas in the DFT method that is carried out in gas phase.

Entire theoretical calculations of ADHPT were worked out by the DFT/B3LYP method with the 6-311++G (d, p) basis set using Gaussian 09 software package [13]. Gauss view molecular visualization program [14] was used to visualize the geometry structure. The theoretical vibrational assignments were interpreted by means of PED (Potential Energy Distribution) using VEDA 4 program [11]. Molecular docking studies give vital details about the orientation of ADHPT (ligand) which regulate the binding affinity between the ligand and their protein target. Molecular docking studies were carried out using Auto Dock 4.2 software [15].

Prediction of Raman intensities

The calculated Raman activities (S_i) were converted to relative Raman intensities (I_i) using the following relations [16]:

$$I_i = \frac{f(\upsilon_0-\upsilon_i)^4 S_i}{\upsilon_i [1 - \exp (hc\upsilon i/k_b T)]} \quad (1)$$

where, υ_0 is the exciting frequency in cm^{-1}, υ_i is the vibrating wavenumber of the i^{th} normal mode, f is a normalization factor for all peak intensities, *h*, c and k_b are Plank's constant, velocity of light and Boltzmann's constant, respectively.

Molecular docking

Molecular docking was employed to elucidate the binding modalities of the investigated ligand towards its target. The three-dimensional structure of human RAS protein was downloaded from the RCSB Protein Data Bank (PDB) with PDB Id 5MLA. The molecular docking program Auto dock 4.2 was used to determine the potential binding mode between the compounds and the selected protein. For the preparation of 5MLA, first crystallographically observed water molecules were eliminated from the protein crystal structure. Then, hydrogen atoms were added using Kollman united atom charges and solvation parameters as provided by Auto Dock Tools [15]. Ligand structures were developed by unifying non-polar atoms of hydrogen, adding Gasteiger partial charges and defining rotatable bonds. A grid box sized 76×74×76 Å was created to conceal the binding site of 5MLA using Auto Grid with points separated by 0.375 Å. The grid box was apportioned for protein using x, y, and z coordinates of 2.765, 25.11 and 39.49, respectively. Docked complexes were pictured and depictions of protein-ligand interactions were engendered using software BIOVIA, Discovery Studio Modeling Environment, Release 4.5 [17].

RESULTS AND DISCUSSION

Molecular geometry

The fundamental structural parameters (bond angles, bond lengths) of the ADHPT values are listed in Table S1 using the B3LYP/6-311G++ (d,p) basis set. In accordance with the atom numbering scheme as obtained from CHEMCRAFT software the optimized structure is shown in Figure 1. The ADHPT has one C-H bond, two C-C bonds, nine C-N bonds, four N-H bonds and one C-S bond. The C-C bond length value of the ring was found to be around 1.396 Å and agrees well with the experimental value of a structurally related compound [1, 2, 18]. The C-H calculated bond length was found to be 1.085 Å and the N-H bond length value was around 1 Å. The C-N bond length values vary from 1.326 to 1.393 Å. The C-S calculated bond length value was 1.659 Å and the experimental value was 1.576 Å. This decrease in bond length may be due to the electronegativity of oxygen atom with neighboring atoms. The bond C-C lengths are greater than C-H bond lengths. The calculated geometries represent a good approximation and they were the bases for calculating vibrational frequencies and thermodynamic properties.

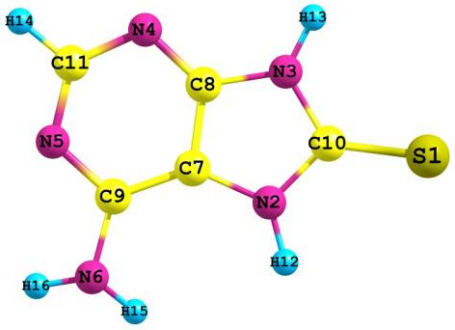

Figure 1. Optimized geometric structure with atoms numbering of ADHPT.

Vibrational assignments

Experimental and theoretical comparative FT-IR and FT-Raman spectra of ADHPT molecule are shown in Figures 2 and 3. The ADHPT molecule consists of 16 atoms, therefore, they have 42 vibrational normal modes. The vibrational frequencies are scaled by 0.961 [12] for B3LYP/6-311++G(d,p) in order to compensate for the errors arising from the basis set incompleteness and neglect the vibrational anharmonicity. The measured (FT-IR and FT-Raman) wavenumbers and assigned wavenumbers values are given in Table S2. They reveal a good correspondence between theory and experiment in the main spectral features.

C-H vibrations

The C-H stretching vibrations are generally identified in the region of 3100-2800 cm^{-1} which is the characteristic region for the ready identification of C-H stretching vibrations [19, 20]. These vibrations are found to be affected by the nature and position of the substituents. In the present study, the IR band was observed at 2854 cm^{-1} and the Raman band at 2976 cm^{-1}. Theoretically computed C-H vibrations values approximately coincide with the experimental values.

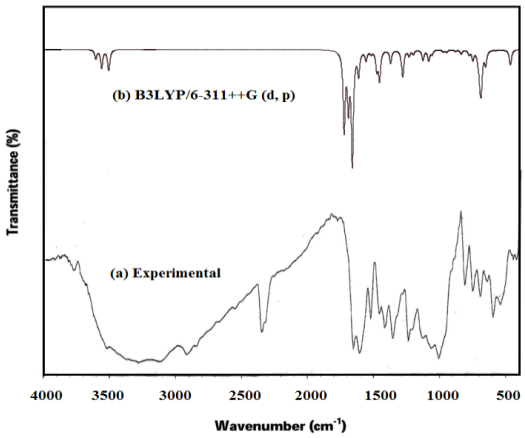

Figure 2. FT-IR spectra of ADHPT (a) Experimental and (b) Theoretical.

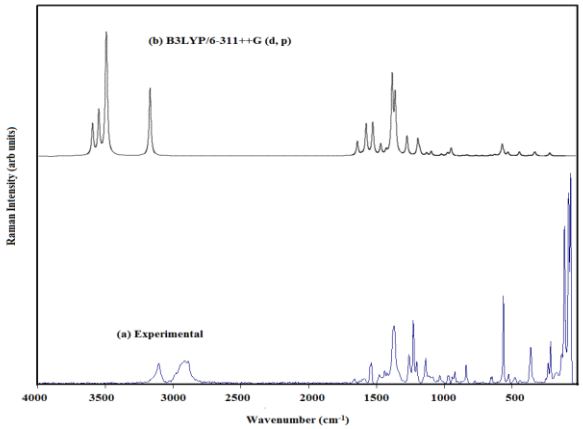

Figure 3. FT-Raman spectra of ADHPT. (a) Experimental and (b) Theoretical.

As indicated by PED, this mode involves 99% of the contribution suggesting that it is a pure stretching mode. The C-H in-plane bending vibrations normally occur as a number of strong- to weak-intensity sharp bands in the region of 1300-1000 cm^{-1} [21] and are very useful for characterization purposes. The bands identified at 1072, 1166, 1230 and 1262 cm^{-1} in the IR spectra and the bending vibrations identified at 1034, 1136, 1209, 1239 and 1268 cm^{-1} in the Raman spectra were assigned to C-H in-plane bending.

C=N and C-N vibrations

The stretching vibrations of C=N occur at 1615-1575 cm^{-1} and those of C-N occur at 1200-1020 cm^{-1} **[**22**].** In this study, the bands identified at 1636, 1482 and 1436 cm^{-1} in the FT-IR spectra and at 1586, 1479, 1440, 1380 and 1372 cm^{-1} in the FT-Raman spectra were assigned to C=N stretching vibrations. For C-N stretching, the bands were identified at 1262, 1230, 1174, 1166 and 1072 cm^{-1} in the FT-IR spectra and at 1268, 1234, 1204 and 837 cm^{-1} in the FT-Raman spectra. The theoretically scaled wave numbers at 1570, 1444, 1431, 1411, 1333, 1312, 1284, 1261 and 1212 cm^{-1} by the DFT method, corresponding to C-N stretching vibrations, coincide with the experimental values with a PED of 57, 58, 59, 62, 63, 69, 73, 77 and 70%, respectively. For C=N stretching vibration, the theoretically scaled wavenumber was at 1570 cm^{-1} with PED of 64%. The remaining vibrations of fundamental modes were also assigned and are listed in Table S2.

Fukui function

Local quantities such as Fukui function and local softness describe the reactivity/selectivity of a specific site in a molecule. The Fukui function is defined in [23]:

$$f_N^+(\boldsymbol{r}) = (\partial\rho(\boldsymbol{r})/\partial N)^+_{v(\boldsymbol{r})} = \rho_{N+1}(\boldsymbol{r}) - \rho_N(\boldsymbol{r}) \quad (2)$$

where, $\rho_{N+1}(r)$ and $\rho_N(r)$ are the electron densities of the N + 1 and N electron systems evaluated at the geometry, v(r), of the N electron system; the superscript plus sign on the derivative indicates that we are considering the derivative from above (right-hand derivative).

The individual atomic charges calculated by Mulliken population analysis (MPA) were used to calculate the Fukui function. Fukui functions $(f^+(\vec{r}), f^-(\vec{r}), f^0(\vec{r}))$, (s_r^+, s_r^-, s_r^0) [22] for all atomic sites in ADHPT are listed in Table 1. Yang and Mortier [24] have given a simple procedure to calculate the atomic condensed Fukui function indices based on MPA and on three possible forward, backward, and central finite difference approximations to the derivatives [25]. Fukui functions were calculated using the following equations:

$$f^+(\vec{r}) = q_r(N+1) - q_r(N) \quad (3)$$

for nucleophilic attack;

$$f^-(\vec{r}) = q_r(N) - q_r(N-1) \quad (4)$$

for electrophilic attack;

$$f^0(\vec{r}) = (q_r(N+1) - q_r(N-1))/2 \quad (5)$$

for radical attack.

In these equations, q_r is the atomic charge (evaluated from Mulliken population analysis, electrostatic derived charge, etc.) at the r^{th} atomic site is the neutral (N), anionic (N+1), cationic (N-1) chemical species.

In Table 1 the values of the Fukui function obtained from the Mulliken charges are reported. From the values reported in Table 1, the reactivity order for the electrophilic case is H_{15}> H_{14}> H_{16}> S_{10}> N_{11}> C_8>H_{13}> H_{12}> N_3. On the other hand, for nucleophilic attack we observe S_{10}>N_5>C_9>H_{13}> N_3>C_2>H_{12}>H_{14}>N_{11}>H_{15}>H_{16}> N_1>N_7>C_4. If one compares the three kinds of attack it may be concluded that the nucleophilic attack is more active in comparison with the electrophilic and radical attack.

HOMO-LUMO energy

The energy gap between HOMO and LUMO is a critical parameter to determine molecular electrical transit properties. HOMO (logical valence bond) can be thought of as the outermost electron containing orbital that tends to give these electrons away as an electron donor or nucleophilic site [26-29].

Table 1. Values of the Fukui function of ADHPT.

Atoms	Mulliken atomic charges			Fukui functions			Local softness		
	0,1 (N)	N +1 (-1, 2)	N-1 (1,2)	fr_+	fr_-	fr_0	sr_+fr_+	sr_-fr_-	$sr_0\ fr_0$
N1	-0.3106	0.0906	-0.2373	0.4012	-0.0733	0.1639	0.0839	-0.0153	0.0343
N3	-0.1268	-0.0317	-0.0913	0.0950	-0.0355	0.0298	0.0199	-0.0074	0.0062
C4	0.3742	-0.6728	0.3917	-1.0470	-0.0175	-0.5323	-0.2189	-0.0037	-0.1113
N5	-0.1636	-0.1604	-0.0931	0.0032	-0.0705	-0.0337	0.0007	-0.0147	-0.0070
C6	0.0991	0.3480	0.1483	0.2489	-0.0492	0.0999	0.0520	-0.0103	0.0209
N7	-0.2416	-0.0974	-0.1723	0.1442	-0.0693	0.0375	0.0302	-0.0145	0.0078
C8	0.0332	-1.7244	0.0415	-1.7576	-0.0083	-0.8829	-0.3675	-0.0017	-0.1846
C9	-0.3150	3.1289	-0.2668	3.4439	-0.0483	1.6978	0.7201	-0.0101	0.3550
S10	-0.6700	-0.7636	-0.3419	-0.0936	-0.3281	-0.2109	-0.0196	-0.0686	-0.0441
N11	-0.3978	-0.3000	-0.3251	0.0979	-0.0728	0.0125	0.0205	-0.0152	0.0026
H12	0.2775	-0.1124	0.3367	-0.3899	-0.0592	-0.2246	-0.0815	-0.0124	-0.0470
H13	0.3410	-0.3449	0.3938	-0.6859	-0.0528	-0.3694	-0.1434	-0.0110	-0.0772
H14	0.1988	0.0561	0.2686	-0.1428	-0.0698	-0.1063	-0.0299	-0.0146	-0.0222
H15	0.2420	-0.6405	0.2684	-0.8825	-0.0264	-0.4545	-0.1845	-0.0055	-0.0950
H16	0.3380	-0.2497	0.3923	-0.5877	-0.0543	-0.3210	-0.1229	-0.0114	-0.0671

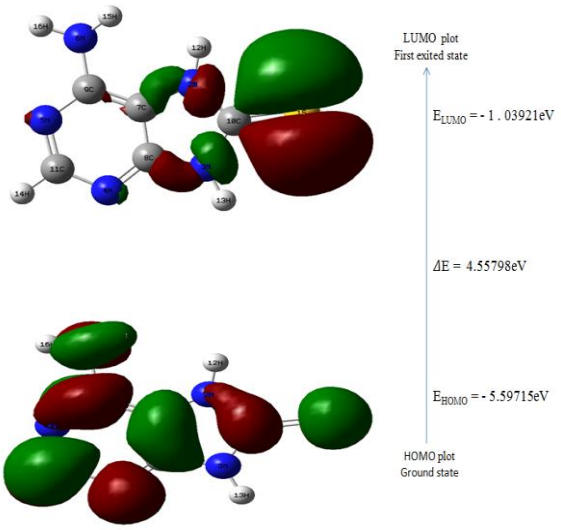

Figure 4. HOMO - LUMO plots of ADHPT.

LUMO (logical conduction band) can be thought of as the innermost orbital containing free sites to electrophilic or accept electrons are of fundamental eminence as it forms the basis of understating the chemical stability and reactivity of a given molecule. The 3D plots of the frontier orbitals HOMO and LUMO figures for the ADHPT are shown in Figure 4.

Pauling introduced the concept of electronegativity as the power of an atom in a molecule to attract electrons to itself. Hardness (η), chemical potential (μ) and electronegativity (χ) and softness (S) are defined as follows:

$$\eta = \frac{1}{2}\left(\frac{\partial_2 E}{\partial N_2}\right)V(r) = \frac{1}{2}\left(\frac{\partial \mu}{\partial N}\right)V(r) \quad (6)$$

$$\eta = \left(\frac{\partial E}{\partial N}\right)V(r)$$

$$\chi = -\mu = -\left(\frac{\partial E}{\partial N}\right)V(r) \quad (7)$$

where, V(r) and E are external potential and electronic energy of an N-electron system, respectively. Softness (S) is a property of molecule that estimates the extent of chemical reactivity. It is the reciprocal of hardness (η).

$$S = 1/2\eta \quad (8)$$

Using Koopman's theorem for closed-shell molecules, η, μ and χ can be defined as:

the hardness of the molecule

$$\eta = (I-A)/2 \quad (9)$$

the chemical potential of the molecule

$$\mu = -(I+A)/2 \quad (10)$$

the electronegativity of the molecule

$$\chi = (A+I)/2 \quad (11)$$

where, I and A are the ionization potential and electron affinity of the molecule, respectively. The ionization energy (I) and electron affinity (A) can be expressed by HOMO and LUMO orbital energies as $I = -E_{HOMO}$ and $A = -E_{LUMO}$. Electron

affinity (A) relates to the efficiency of a ligand to accept in particular one electron from a donor. The ionization potential calculated by the B3LYP/6-311++G (d,p) method for ADHPT is 5.59715 eV. Considering the chemical hardness, large frontier orbital gap (HOMO–LUMO) means a hard molecule and small frontier orbital gap (HOMO–LUMO) means a soft molecule. A molecule with small frontier gap is generally associated with a low kinetic stability and high chemical reactivity. Recently Parr *et al.* [26] have defined a new descriptor electrophilicity index (ω), which describes a quantitative classification of the global electrophilic nature of a molecule. They defined the electrophilicity index (ω) as follows:

$$\omega = \mu^2/2\eta \qquad (12)$$

Using the above equations, the chemical potential, hardness and electrophilicity index were calculated for ADHPT and their values are shown in Table 2. The usefulness of this new reactivity quantity has been recently proved in understanding the toxicity of various pollutants concerning their site selectivity and reactivity [30-31]. The calculated value of the electrophilicity index describes the biological activity of ADHPT.

Molecular Electrostatic Potential (MEP)

The three-dimensional MEP of ADHPT is illustrated in Figure 5. The MEP is related to the electronic density which is a very useful descriptor for determining the sites for electrophilic attack and nucleophilic reactions, as well as hydrogen-bonding interactions [32, 33]. MEP clearly exhibits molecular size, shape in terms of color grading.

Table 2. Calculated energy values of ADHPT.

Basis set	B3LYP/6-311++G(d, p)
E_{HOMO}(eV)	-5.59715
E_{LUMO}(eV)	-1.03921
Ionization potential	5.59715
Electron affinity	1.03921
Energy gap(eV)	4.55794
Electronegativity	3.31818
Chemical potential	-3.31818
Chemical hardness	2.27897
Chemical softness	0.21940
Electrophilicity index	2.41564

As can be seen from the MEP of the title compound, while the regions having negative potential are over the electronegative atoms (nitrogen and sulfur), the regions having positive potential are the hydrogen atoms. From this result, we can conclude that the hydrogen atom indicates the strongest repulsion and nitrogen and sulfur atoms indicate the attraction.

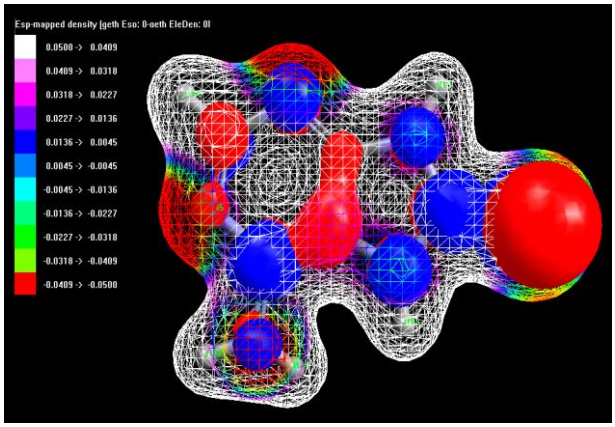

Figure 5. MEP on ADHPT.

Molecular docking

The low toxicity levels of ADHPT calculated in terms of the softness value and the electrophilicity index that act as a biological descriptor, led to molecular docking investigations.

Molecular docking was performed against 5MLA and its purpose was to estimate the binding modalities of ADHPT. Hydrogen bonding plays an important role in the structure and function of biological molecules, the ligand-receptor interactions were inspected on the basis of hydrogen bonding. Table 3 shows the corresponding binding energy, interactions, distance and bonding type. It is evident from Table 3 that the ligand molecule ADHPT is tightly fitted with the active position of 5MLA with very good binding energy - 5.99 kcal/mol, as shown in Figure 6.

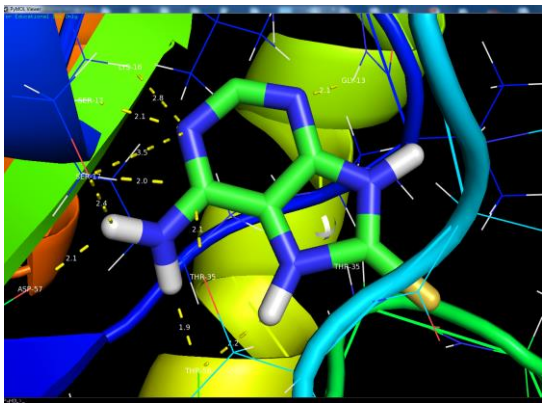

Figure 6. Docking and hydrogen bond interaction of ADHPT with 5MLA.

In molecular docking, the actual requirement is not to find out only RMSD and binding energy values. The molecular interactions like hydrogen bonds, hydrophobic interactions, van der Waal interactions, ionic bonds, etc. are also playing important roles. So, based on RMSD and binding energy the selection of a compound or ligand is not a true way. In some cases, it is possible that the best pose has good binding energy due to the presence of more hydrophobic and van der Waal interactions but it does not contain the stronger hydrogen bond while in the next pose 3-7 hydrogen bonds are present and there are less hydrophobic and van der Waal interactions compared to the best pose. So, in this case the binding energy of the first best pose is -5.43 kcal/mol and of the second is -5.99 kcal/mol. In this way, the second pose is superior because of stronger hydrogen bond interaction between protein and ligand. The docked poses for each controlled inhibitor were evaluated and the pose with the lowest binding free energy and inhibition constant was thereby chosen. The lowest binding free energy (i.e. best docking score) and inhibition constant indicated the highest ligand/protein affinity.

The hydrogen bond lengths and binding energies of the title molecule with different proteins were identified. A minimum binding energy of -5.99 kcal/mol was found for the interaction of protein 5MLA with the bonded residues GLY13, LYS16, SER17, ASP57 and THR58.

Table 3. Molecular docking with 5MLA.

Protein (PDB ID)	Bonded residues	No. of hydrogen bonds	Bond distance (Å)	Estimated inhibition constant (μm)	Binding energy (kcal/mol)	Torsional free energy
5MLA	GLY13	7	2.1	40.45	-5.99	0.3
	LYS16		2.8			
	SER17		2.1			
	SER17		3.5			
	ASP57		2.1			
	THR58		2.2			
	THR58		1.9			

CONCLUSION

In this investigation, the optimized parameters of title compound structure were found at B3LYP/6-311++G (d,p) level of theory. Comparisons between theoretical and experimental geometrical parameters showed that DFT calculations were in good compatibility with experimental results. The vibrational FT-IR and FT-Raman spectra of the ADHPT molecule were recorded and on the basis of agreement between the calculated and experimental results, the assignments of all fundamental vibrational modes of ADHPT were made unambiguously based on the results of the PED. Low HOMO–LUMO energy gap value indicates that intramolecular charge-transfer takes place within the molecule. Fukui function helps to identify the electrophilic/ nucleophilic nature of a specific site within a molecule. The MEP shows that negative potential sites are on nitrogen and sulfur atoms while the positive potential sites are around the hydrogen atoms. This study shows clearly the inhibitor effect, based on binding affinities and interactions formed between amino acid residues and candidate molecules, of the title compound in front of microbial enzymes. The interactions between the molecule and the antimicrobial enzyme are dominated by van der Waals and hydrogen bond interactions.

The protein-ligand interactions (hydrogen bonds and hydrophobic contacts) and binding energy score enhance the medicinal activity of the ligand. Hence, the title compound may be deemed as an effective and suitable inhibitor of antibacterial diseases.

Acknowledgement: *The authors thank Dr. Babu Vargheese, SAIF, IIT, Chennai, India, for his help with the data collection.*

REFERENCES

1. S. Gunasekaran, S. Kumaresan, R. Arunbalaji, G. Anand, S. Seshadri, S. Muthu, *J. Raman Spectrosc.* **40(11)**, 1675 (2009).
2. I. N. Latosinska, J. Seliger, V. Zagar, D. V. Burchardt, *Journal of Physical Chemistry* **A, 113.30**, 8781 (2009).
3. S. Sahasranaman, D. Howard, S. Roy, *Eur. J. Clin. Pharmacol*., **64(8)**, 753 (2008).
4. L. Lennard, John S. Lilleyman, *J. Clin. Oncol.* **7(12)**, 1816 (1989).

5. N. Issaeva, *J. Cancer Res.,* **70(15)**, 6268 (2010).
6. D. A. Dougherty, *Science*, **271**, 163 (1996).
7. P. Hohenberg, W. Kohn, *Phys. Rev.,* **136** B, 864 (1964).
8. A. D. Becker, *J. Chem. Phys.*, **98,** 5648 (1993).
9. C. Lee, W. Yang, R. G. Parr, *Phys. Rev.*, **B37**, 785 (1988).
10. A. Frisch, A.B. Nielsen, A. J. Holder, Gauss View User's Manual, Gaussian Inc., Pittsburg, PA, 2000.
11. M. H. Jamroz, Vibrational Energy Distribution Analysis VEDA 4 program, Warsaw, 2004.
12. V. Vetrivelan, *J. Nanosci. Tech*. **4**, 348 (2018).
13. M. J. Frisch, Gaussian 09, Gaussian Inc., Wallingford, CT, USA, 2009.
14. R. Dennington, T. Keith, J. Millam, Gauss View, Version 4.1.2, Semichem Inc., Shawnee mission, KS, 2007.
15. G. Morris, R. Huey, W. Lindstrom, M. Sanner, R. Belew, D. Goodsell, A. Olson, *J. Comput. Chem*., **30** (16), 2785 (2009).
16. G. Keresztury, Raman spectroscopy: Theory in Handbook of vibrational spectroscopy, 2002.
17. Discovery Studio, 'Dassault Systèmes BIOVIA, Discovery Studio Modeling Environment', Release 4.5, San Diego, Dassault Systèmes, 2015.
18. C. E. Bugg, U. Thewalt, *Acta Crystallogr. Sect. A.*, **31(1)**, 121 (1975).
19. S. Bourcier, Y. Hoppilliard, *Int. J. Mass Spectrom.*, **217(1)**, 231 (2002).
20. Y. Yu, L. Ke, X. Zhou, H. Wang, Sh. Liu, X. Ma, *J. Phys. Chem. A*, **111,** 8971 (2007).
21. G. Socrates, Infrared and Raman Characteristics Group Frequencies, Third edn., Wiley, New York, 2001.
22. L. J. Bartolotti, P. W. Ayers, *J. Phys. Chem*. A, **109**, 1146 (2005).
23. P. K. Chattaraj, Chemical Reactivity Theory: A DFT View. CRC Press, (2009).
24. W. Yang, W. J. Mortier, *J. Am. Chem. Soc.*, **108,** 5708 (1986).
25. O. Christiansen, J. Gauss, J. F. Stanton, *J. Chem. Phys. Lett*., **305**, 147 (1999).
26. R. G. Parr, L. Szentpaly, S. Liu, *J. Am. Chem. Soc*., **121**, 1922 (1999).
27. P. K. Chattaraj, B. Maiti, U. Sarkar, *J. Phys. Chem.*, **A107**, 4973 (2003).
28. R. G. Parr, R. A. Donnelly, M. Levy, W. E. Palke, *J. Chem. Phys.*, 6**8**, 3801 (1978).
29. R. G. Parr, R. G. Pearson, *J. Am. Chem. Soc.*, **105,** 7512 (1983).
30. R. G. Parr, P. K. Chattraj, *J. Am. Chem. Soc.*, **113**, 1854 (1991).
31. R. Parthasarathi, J. Padmanabhan, M. Elango, V. Subramanian, P. Chattaraj, *Chem. Phys. Lett.*, **394**, 225 (2004).
32. P. Politzer, J. S. Murray, *Theor. Chem. Acc.*, **108**, 134 (2002).
33. E. Scrocco, J. Tomasi, *Adv. Quantum Chem.*, **11**, 115 (1978).